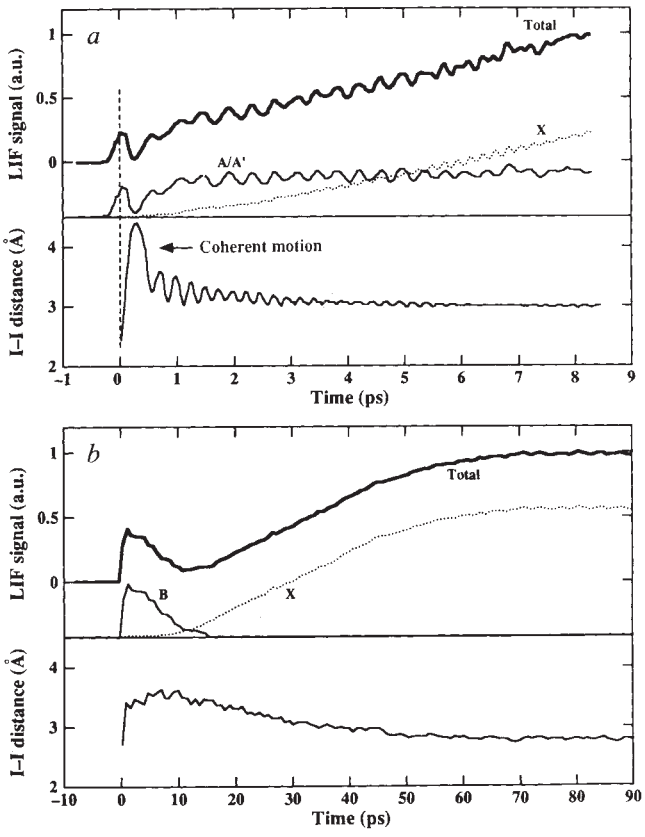

FIG. 4 Laser-induced fluorescence signals and internuclear separation calculated from molecular dynamics simulations. *a*, Simulated transients of $I_2 \cdot Ar_{44}$ when iodine is excited to the A state above its dissociation limit by a pump wavelength of 614 nm. The dotted line is the contribution from recombination on the ground state X. The thin solid line comes from recombination on the A/A state. The thick solid line is the sum (see text). *b*, Simulated transients with pump wavelength tuned to 510 nm which excites the B state. The thin solid line represents signal from B state, while the dotted line represents contributions from the X state. The thick solid line is the sum. For both A- and B-state dynamics, the intrinsic change of the I–I distance with time is shown. Note the dramatic change in the motion on A potential compared to the B potential, and that the coherent motion is evident only in the A-state dynamics. The simulations invoke classical mechanics and the persistence of some oscillations up to 9 ps might disappear in a quantum calculation[27].

range nature of the interaction with the solvent, while for ionic systems the long-range Coulomb interaction dominates. As with isolated chemical reactions[3] such studies of coherent nuclear motions[24,31,32] in complex systems of solvent cages allow for resolution of the dynamics on the timescale of atomic motion. □

Received 22 April; accepted 7 July 1993.

1. Frank, J. & Rabinovitch, E. *Trans. Faraday Soc.* **30,** 120–131 (1934).
2. Porter, G. & Smith, J. A. *Proceedings Royal Soc.* A **261,** 28–37 (1961).
3. Zewail, A. H. *Faraday Discuss. Chem. Soc.* **91,** 207–237 (1991).
4. Saenger, K. L., McClelland, G. M. & Herschbach, D. R. *J. phys. Chem.* **85,** 3333–3337 (1981).
5. Jortner, J., Scharf, D., Ben-Horin, N., Evan, U. & Landman, U. in *Proc. int. School of Physics* (ed. Scholes, G.) 43–98 (North-Holland, Amsterdam, 1990).
6. Berry, R. S. in *Proc. int. School of Physics* (ed. Scholes, G.) 3–22 (North-Holland, Amsterdam, 1990).
7. Papanikolas, J. M. *et al. J. phys. Chem.* **95,** 8028–8040 (1991).
8. Breen, J. J. *et al. J. chem. Phys.* **92,** 805–807 (1990).
9. Gutmann, M., Willberg, D. M. & Zewail, A. H. *J. chem. Phys.* **97,** 8048–8059 (1992).
10. Potter, E. D., Liu, Q. & Zewail, A. H. *Chem. Phys. Lett.* **200,** 605–614 (1992).
11. Papanikolas, J. M. *et al. J. chem. Phys.* **97,** 7002–7005 (1992).
12. Baumert, T., Engel, V., Meier, C. & Gerber, G. *Chem. Phys. Lett.* **200,** 488–494 (1992).
13. Wei, S., Purnell, J., Buzza, S. A., Stanley, R. J. & Castleman, A. W. Jr *J. chem. Phys.* **97,** 9480–9482 (1992).
14. Schreiber, E., Kühling, H., Kobs, K., Rutz, S. & Wöste, L. *Ber. Bunsenges. phys. Chem.* **96,** 1301–1305 (1992).
15. Amar, F. G. & Berne, B. J. *J. phys. Chem.* **88,** 6720–6727 (1984).
16. Alimi, R., Gerber, R. B., McCaffray, J. G., Huntz, H. & Schwentner, N. *Phys. Rev. Lett.* **69,** 856–859 (1992).
17. Stace, A. J. *J. Chem. Soc. Farad. Trans. II* **77,** 2105–2110 (1981).
18. Fei, S., Zheng, X., Heaven, M. & Tellinghuisen, J. *J. chem. Phys.* **97,** 6057–6063 (1992).
19. Valentini, J. J. & Cross, J. B. *J. chem. Phys.* **77,** 572–573 (1982).
20. Beswick, J. A., Monot, R., Phillippoz, J.-M. & van den Bergh, H. *J. chem. Phys.* **86,** 3965–3967 (1987).
21. Burke, M. L. & Klemperer, W. *J. chem. Phys.* **98,** 1797–1809 (1993).
22. Schroeder, J. & Troe, J. *A. Rev. phys. Chem.* **38,** 163–190 (1987).
23. Harris, A. L., Brown, J. K. & Harris, C. B. *A. Rev. phys. Chem.* **39,** 341–366 (1988).
24. Scherer, N. F., Ziegler, L. D. & Fleming, G. R. *J. chem. Phys.* **96,** 5544–5547 (1992).
25. Dardi, P. S. & Dahler, J. S. *J. chem. Phys.* **98,** 363–372 (1993).
26. Bowman, R. M., Dantus, M. & Zewail, A. H. *Chem. Phys. Lett.* **161,** 297–302 (1989).
27. Gruebele, M. & Zewail, A. H. *J. chem. Phys.* **98,** 883–902 (1993).
28. Farges, J., de Ferandy, M. F., Raoult, B. & Torchet, G. *J. chem. Phys.* **84,** 3491–3501 (1986).
29. Tellinghuisen, J. *J. chem. Phys.* **58,** 2821–2834 (1973).
30. Nesbit, D. J. & Hynes, J. T. *J. chem. Phys.* **77,** 2130–2143 (1982).
31. Joly, A. G., Ruhman, S., Kohler, B. & Nelson, K. A. *Springer Ser. chem. Phys.* **48,** 506–510 (1988).
32. Benjamin, I., Banin, U. & Ruhman, S. *J. chem. Phys.* **98,** 8337–8340 (1993).

ACKNOWLEDGEMENTS. This work was supported by a grant by the National Science Foundation.

Template mineralization of self-assembled anisotropic lipid microstructures

Douglas D. Archibald & Stephen Mann*

School of Chemistry, University of Bath, Bath BA2 7AY, UK

THE high-fidelity replication and functional specificity of biomaterials and biopolymers is inspiring a renewal in the development of biomimetic strategies for materials synthesis[1,2]. Approaches involving the templating or nucleation of inorganic materials by compressed monolayers of amphiphiles[3–5], the use of supramolecular lipid or protein cages in the preparation of nanoscale inorganic structures[6–8] and the mineralization of bacterial fibres[9] indicate the potential of controlled crystallization at inorganic–organic interfaces. Here we report the controlled formation of tubular inorganic–organic composites by using self-assembled lipid tubules as templates for the crystallization of inorganic oxides. We use microstructures formed by a sugar-based lipid galactocerebroside, doped with small amounts of an anionic sulphated derivative, to induce nucleation of magnetic and non-magnetic iron oxides. By varying the reaction conditions, we can create either tube-like or lamellar disk-like composites. Our results suggest that the variety of microstructures formed by chemically modified sugar-based lipids may provide a route to the production of mineral-containing fibres and other ceramic–organic composites.

To prepare oriented mineralized microstructural units that can be processed into higher-order assemblies, isotropic amphiphilic structures such as Langmuir monolayers (in two dimensions) and vesicles (in three) are of limited use—what one needs are anisotropic structures such as tubes or fibres. Self-assembled lipid tubules[10] with large axial-ratios have been observed in systems containing semisynthetic chiral amphiphiles[11], amino-acid-based surfactants[12,13], sugar-based surfactants[14] and biological galactocerebrosides[15]. Recent studies have shown that tubules containing phosphatidylcholine headgroups could be metallized with electroless nickel[16], coated in preformed colloidal silica[17], or mineralized with a metal carbonate by chemical precipitation[18]. The latter process, although based on surface chemical interactions, was not highly specific to the organic sur-

* To whom correspondence should be addressed.

face. Here we describe the chemical tailoring of a newly discovered large axial-ratio lipid microstructure to produce nucleation sites for the synthesis of inorganic–organic composites of anisotropic (fibrous) morphology. Our approach is outlined in Fig. 1. Mixtures of galactocerebrosides such as α-hydroxy fatty acid galactocerebroside (HFA-Cer) and non-hydroxy fatty acid galactocerebroside (NFA-Cer) form a range of microstructures (I, II and III in Fig. 1) depending on lipid composition (Fig. 1*b*). The details of these microstructures and phase relationships are described in detail elsewhere[19]. These microstructures are activated for inorganic mineralization by the incorporation of low levels of anionic sulphated galactocerebroside (S-Cer, sulphatide) into the neutral lipid microstructures of HFA-Cer and NFA-Cer, without significant disruption of their morphologies[19].

Lipid cylinders of variable composition were prepared by thermal-mechanical cycling of 1.5 mg ml^{-1} suspensions of mixtures (% by weight) of bovine brain HFA-Cer (Sigma) and bovine brain S-Cer (Lipid Products) in ethylene glycol as described[15,19]. The cylinders were open-ended multilamellar tubules with a diameter of ~120 nm and a central lumen of 10–30 nm (Fig. 2*a*). Aliquots (40 cm^3) of the lipid suspension in ethylene glycol were incubated with 4–100 cm^3 of freshly prepared 10 mM $FeCl_3$ in 0.10 mM HCl at room temperature, under air. The best conditions for specific mineralization of the tubules were found to be: 0.9 mM $FeCl_3$, 1 mM HCl and 0.06 mM of 90% HFA-Cer : 10% S-Cer). Mineralization resulted in the slow appearance of an orange colour, coagulation, and sedimentation of the coated lipid tubules. Significantly, controls without iron did not cause lipid coagulation or sedimentation, and microstructures not doped with S-Cer (that is 100% HFA-Cer) sedimented at a slower rate and did not develop the orange colour.

The mineralized tubules were covered in granular and sheet-like material (Fig. 2*b*) which gave peaks for oxygen, sulphur and iron by energy dispersive X-ray analysis. Selected-area electron diffraction patterns recorded on individual tubules indicated that the inorganic coating was poorly crystalline lepidocrocite (γ-FeOOH) (d_{hkl}: 0.331 nm (120), 0.254 nm (031), 0.242 nm (111)

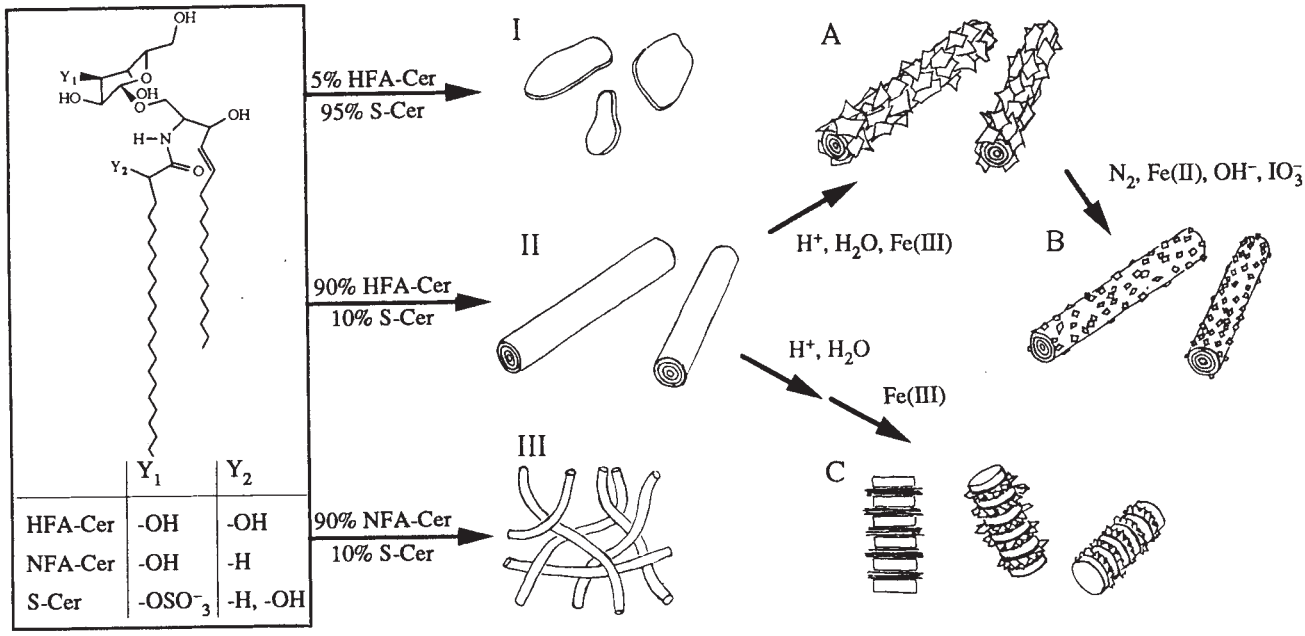

FIG. 1 *a*, Generalized scheme for the introduction of shape anisotropy in biomimetic inorganic–organic composites. Galactocerebroside mixtures can produce a variety of microstructures in ethylene glycol suspension: I, lamellar disks; II, multilamellar tubules; III, Viscoelastic gel of fibrous unilamellar tubules. In synthetic route A, a cylindrical coating of γ-FeOOH (lepidocrocite) is generated by incubation of microstructures II in a solution of acidic Fe(III). Synthesis B illustrates that the γ-FeOOH on these tubules can be subsequently converted *in situ* to a ferrimagnetic inverse spinel material (magnetite or maghemite) by room temperature anaerobic reaction with stoichiometric amounts of Fe(II)[21]. In both routes, hydration of the bilayer tubule structures is retarded by binding of Fe(III) and iron oxides, but if route C is followed, S-Cer-rich lamellar disks separate from the parent microstructures by suspension in acidic water before addition of Fe(III). Subsequent binding of Fe(III) by these disks results in growth of oriented thin plates of γ-FeOOH crystals intercalated between the lipid lamellae. *b*, Diagrammatic summary of phase behaviour exhibited in mixtures of the lipids α-hydroxy fatty acid galactocerebroside (HFA-Cer), non-hydroxy fatty acid galactocerebroside (NFA-Cer) and anionic sulphated galactocerebroside (S-Cer). Each corner of the diagram describes the microstructures produced by the pure lipid prepared by slow cooling of glycol suspensions at 100 °C. LB = lamellar blebs; LD = lamellar disks; ULC = unilamellar cylinders; MLC = multilamellar cylinders; HMLC = helically patterned multilamellar cylinders; HMLR = helical multilamellar ribbons; MLCC = multilamellar cochleate cylinders. Numbers in parentheses are typical lumen diameters.

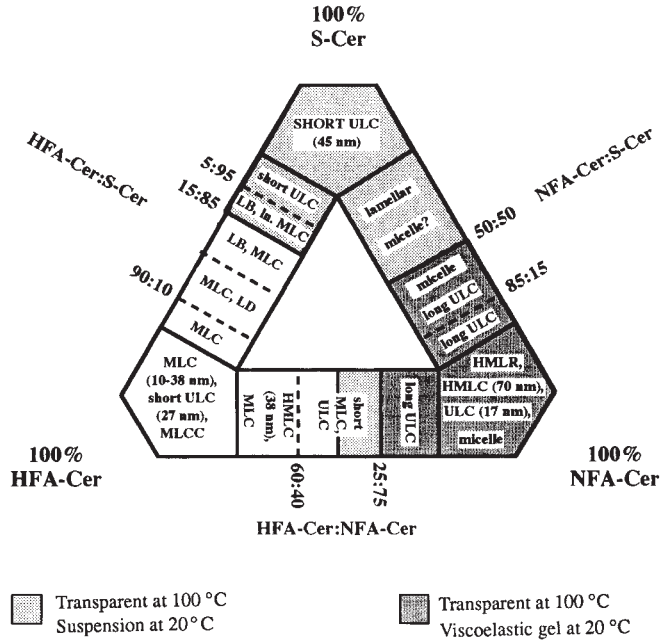

and 0.121 nm (222)) with a small fraction of ferrihydrite ($Fe_2O_3 \cdot nH_2O$). The sheet-like material was identified as γ-FeOOH by high resolution lattice images which clearly showed a 0.66 nm spacing (d_{hkl} (020)). FT-infrared spectroscopy of the lipid-mineral composite showed the 740 cm^{-1} characteristic band of lepidocrocite (data not shown). Infrared spectroscopy also gave results which implied that the hydrocarbon and amide functionalities were largely unchanged within the molecular structure associated with the mineralized tubules, whereas the galactosyl interface was partially modified due to the presence of iron oxyhydroxide and/or water of hydration.

Conversion of lepidocrocite coated tubules *in situ* was carried out under nitrogen, at room temperature and with minimal stirring. A small volume of deaerated $(NH_4)_2SO_4 \cdot Fe(II)SO_4 \cdot 6H_2O$ solution was added to a suspension of the Fe(III) mineral-coated tubules to give a 1 : 1 molar ratio of Fe(II) : Fe(III). The phase transformation reaction was then initiated by addition of 100 mM NaOH to raise the pH to 8.5. In some experiments, iodate (IO_3^-) was also added as an oxidant to produce tubules extensively mineralized with crystals of poorly-ordered geothite (α-FeOOH) (Fig. 3*a*). In other experiments, the reaction mixture was maintained at pH 8–9 by additional aliquots of NaOH and left for 4 days. A black tubule-containing precipitate, which was responsive to the field of a bar magnet, was isolated. Electron microscopy images showed that the lipid tubules were encrusted with clusters of fine-grained inorganic material (Fig. 3*b*) which was identified by electron diffraction (d_{hkl}: 0.479 nm (111), 0.300 nm (220)) as the ferrimagnetic inverse spinel phase magnetite (Fe_3O_4). The electron diffraction data were not sufficient to distinguish this mineral from the oxidized ferrimagnetic spinel, maghemite (γ-Fe_2O_3).

Different results were obtained if a S-Cer-doped lipid tubule suspension in ethylene glycol was incubated for 10 min in acid solution before addition of Fe(III) (route C, Fig. 1). This produced a S-Cer-rich phase which was observed by TEM to be formed by partial phase separation from the parent tubules. Subsequent Fe(III) addition caused aggregation of the segregated anionic lipid into stacks of lamellae, interspaced with nanometre-thin layers of poorly-crystalline iron oxyhydroxide. Presumably, Fe(III) binds preferentially to the surface of the disks because of their high negative charge, and the concomitant neutralization of surface charge gives rise to stack formation. The initial mineral was transformed over a period of weeks into sheet-like crystals of lepidocrocite which were aligned by confinement between the stacked lipid lamellae (Fig. 3*c*). The stacked disk nanocomposite was also produced directly in pure S-Cer controls but the product was less well-defined (data not shown). As the disks are ~6.5 nm thick, the mineralized system is a nanocomposite of inorganic and organic layers. Although more structural work is required to determine the details of this association, it is possible that organized stacks of inorganic–organic materials could be of potential significance in the catalytic, photochemical and electronic application of finely divided solids.

Our results indicate that high axial ratio inorganic–organic composites can be routinely produced by template mineralization of chemically-modified galactocerebroside tubules. Incorpo-

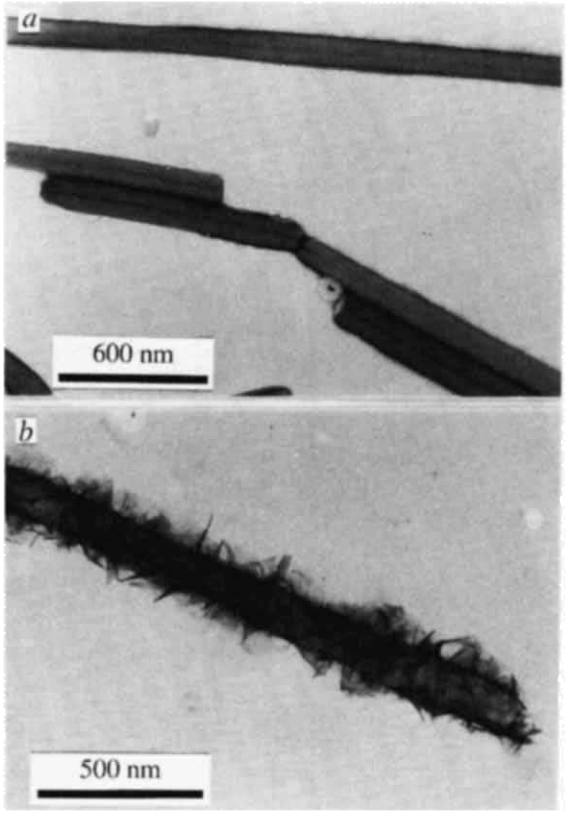

FIG. 2 Transmission electron micrographs of lipid tubules and mineralized products. *a*, Lipid tubules formed from a mixture of 90% HFA-Cer and 10% S-Cer prior to mineralization. *b*, Mineralization with lepidocrocite by synthetic route A (Fig. 1*a*).

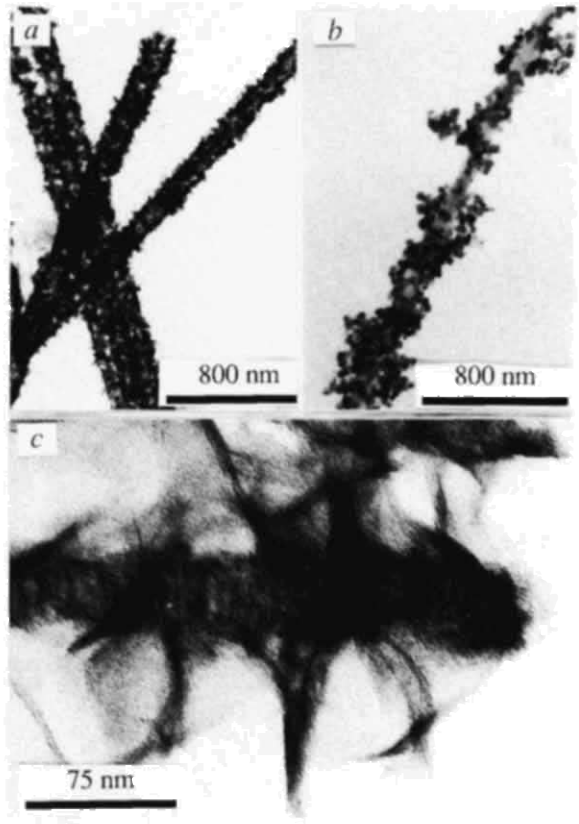

FIG. 3 Transmission electron micrographs of lipid-mineral composites after *in situ* conversion reactions. *a*, α-FeOOH encrusted tubules (90% HFA-Cer, 10% S-Cer) formed by secondary oxidation of Fe(II) on the surface of γ-FeOOH coated fibres. *b*, Magnetic tubules formed by reaction of γ-FeOOH coated fibres (90% HFA-Cer, 10% S-Cer) with Fe(II) under N_2 to give magnetite (Fe_3O_4). *c*, Crystals of lepidocrocite grown between 6.5 nm lamellar lipid disks formed by acid conversion of unmineralized tubules (90% HFA-Cer, 10% S-Cer) before addition of Fe(III). Image is of an unstained sample. Intra-stack crystals (dark parallel lines) and sheet-like lepidocrocite overgrowths can be observed.

ration of sulphatide into the neutral galactocerebroside assemblies gives the microstructure anionic sites for electrostatic binding of Fe(III) polyhydroxy cationic species (which are formed at low pH[20]). These binding sites are the initial foci for nuclei formation such that, under optimal structural and solution conditions, inorganic deposition is confined to the tubule surface. In the case of iron oxide mineralization, no preferential crystallographic orientation with respect to the lipid microstructure was observed, although this does not rule out the possibility of oriented nucleation with more crystalline minerals such as $CaCO_3$ and $BaSO_4$. Moreover, the presence of the iron mineral coating stabilizes the lipid microstructure with respect to hydration so that suspension of the high axial ratio composites can undergo chemical transformations; for example, to produce magnetic tubules. A range of inorganic–organic materials could conceivably be synthesized by this route. We have observed, however, that although amorphous calcium phosphate has a high nucleation affinity for S-Cer-doped HFA-Cer tubules, subsequent phase transformation to crystalline hydroxyapatite is often not associated with the lipid surface (D. Walsh and S.M., unpublished data). Thus, the interplay between interfacial and solution chemistry is critical in dictating the nucleation specificity of these inorganic–organic interfaces.

Finally, we note that although we have been successful in promoting inorganic nucleation on the external surface of the lipid microstructure, we have not yet been able to synthesize reproducibily tubule-based composites in which the inorganic phase resides solely within the 10–30 nm central lumen of the supramolecular assembly. The synthesis of organic-lined inorganic filaments, as well as the production of viscoelastic gels of mineralized S-Cer-doped NFA-Cer unilamellar tubules (Fig. 1, route III) are the principal objectives of current and future work. □

Received 24 February 1993; accepted 14 June 1993.

1. Heuer, A. H. *et al. Science* **225,** 1098–1105 (1992).
2. Mann, S. *et al. MRS bulletin* **XVII(10),** 32–36 (1992).
3. Mann, S., Heywood, B. R., Rajam, S. & Birchall, J. D. *Nature* **334,** 692–695 (1988).
4. Zhao, X. K., Yang, J., McCormick, L. D. & Fender, J. H. *J. phys. Chem.* **96,** 9933–9938 (1992).
5. Gavish, M., Popovitz-Biro, R., Lahav, M. & Leiserovitz, L. *Science* **250,** 973–974 (1990).
6. Meldrum, F. C., Wade, V. J., Nimmo, D. L., Heywood, B. R. & Mann, S. *Nature* **349,** 684–687 (1991).
7. Meldrum, F. C., Heywood, B. R. & Mann, S. *Science* **257,** 522–523 (1992).
8. Mann, S., Hannington, J. P. & Williams, R. J. P. *Nature* **324,** 565–567 (1986).
9. Mendelson, N. H. *Science* **258,** 1633–1636 (1992).
10. Ekwall, P. *Adv. Liq. Cryst.* **1,** 1–142 (1975).
11. Yager, P. & Schoen, P. E. *Molec. Cryst. liq. Cryst.* **106,** 371–381 (1984).
12. Yamada, K., Ihara, H., Ide, T., Fukumoto, T. & Hirayama, C. *Chemy Lett.* 1713–1716 (1984).
13. Nakashima, N., Asakuma, S., Kim, J. M. & Kunitake, T. *Chemy Lett.* 1709–1712 (1984).
14. Fuhrhop, J. H., Schneider, P., Rosenberg, J. & Boekema, E. *J. Am. chem. Soc.* **109,** 3387–3390 (1987).
15. Archibald, D. D. & Yager, P. *Biochemistry* **31,** 9045–9055 (1992).
16. Schnur, J. M. *et al. Thin Solid Films* **152,** 181–206 (1987).
17. Baral, S. & Schoen, P. *Chem. Mat.* **5,** 145–147 (1993).
18. Chappel, J. S. & Yager, P. *J. Mat. Sci. Lett.* **11,** 633–636 (1992).
19. Archibald, D. D. & Mann, S. *Chem. Phys. Lipids* (in the press).
20. Henry, M., Jolivet, J. P. & Livage, J. *Struct. and Bonding* **77,** 168–178 (1992).
21. Tamaura, Y., Ito, K. & Katsura, T. *J. chem. Soc. Dalton Trans.* 189–194 (1983).

ACKNOWLEDGEMENTS. We gratefully acknowledge the financial support of the Science and Engineering Research Council.

Large igneous province on the US Atlantic margin and implications for magmatism during continental breakup

W. S. Holbrook & P. B. Kelemen

Woods Hole Oceanographic Institution, Woods Hole, Massachusetts 02543, USA

RIFTED continental margins commonly include sections of igneous rock more than twice as thick as normal oceanic crust. Explanations for this voluminous magmatic accretion during rifting include plume models[1–3], which require a deep-seated thermal or chemical anomaly in upwelling mantle, and non-plume models[4–7], which call on broad, shallow thermal anomalies and/or rapid upwelling of mantle through the melting zone. New seismic models from two transects across the continent–ocean transition on the US Atlantic margin[8–10] confirm the presence of a 20–25-km-thick igneous section. Here we argue that the similarity of the crustal structure on these and two previous transects, spanning 1,000 km of the margin, and the association of thick igneous crust with the East Coast magnetic anomaly[11] imply that the thick igneous section extends along the entire margin and may have a volume of as much as 3.2×10^6 km^3. The distribution of volcanic and plutonic rocks, details of the seismic structure, and lack of independent evidence for a hotspot are difficult to reconcile with plume models and suggest that non-plume processes created the thick igneous crust.

Studies of the continental margins of the North Atlantic have shown that voluminous igneous activity, on a scale rivalling the largest continental flood basalt provinces, accompanied the onset of sea-floor spreading[1,12]. Igneous activity on these 'volcanic margins' is shown in seismic data as seaward-dipping reflections beneath the post-rift unconformity on multichannel seismic reflection (MCS) data[13,14], and thick, high-seismic-velocity (P-wave velocity 7.2–7.5 km s^{-1}) lower crust interpreted from wide-angle seismic data[1,12]. Other margins (such as the Iberia margin), appear to be 'non-volcanic', as evidenced by lower seismic velocities (6.3–6.6 km s^{-1}) in the lower crust, lack of seaward-dipping reflections, and block-faulted basement interpreted as thinned continental crust[15,16].

The first indications of significant volumes of volcanic material in the crust of the eastern margin of the United States came from seaward-dipping reflections on MCS data[17] and high velocity (7.2–7.5 km s^{-1}) lower crust interpreted from wide-angle seismic data in the Baltimore Canyon[18] and Carolina Troughs[19] (Figs 1, 2). Tréhu *et al.*[19] inferred that the margin was volcanic. Due to limited resolution of those data sets, however, the full thickness and extent of igneous rocks was uncertain, and White and McKenzie[20] concluded that the margin was only mildly volcanic and formed at the distal edge of a hotspot.

Improved images of the geometry and distribution of rift-related igneous rocks have resulted from joint MCS and wide-angle seismic experiments conducted recently in the Carolina and southern Baltimore Canyon troughs[8–10] (Fig. 1). The resulting images show well-developed seaward-dipping reflections together with a thick, high-velocity lower crust (Figs 3, 4). Beneath the seaward-dipping reflections, deep reflections from the Appalachian crust disappear, the Moho shows a striking change in reflective character (Fig. 3), and seismic velocities increase rapidly (Fig. 4). These abrupt lateral changes indicate that very little continental material persists beneath the volcanic wedge, so that the crust there consists almost entirely of new igneous material. The US Atlantic margin is therefore strongly volcanic at least from the Blake Spur fracture zone to offshore New Jersey, and probably along its entire length, as discussed below. The thickness of igneous material added to the crust reaches 25 km in the BA-6 and EDGE transects, exceeding the 18.5 km thickness interpreted on the Hatton Bank[21], which was within 600–700 km of the Iceland hotspot during rifting. Although the inferred igneous material on the US Atlantic margin is buried beneath thick post-rift sediments and is therefore difficult to